10. Pacini F, Gasperi M, Fugazzola L, et al. Testicular function in patients with differentiated thyroid carcinoma treated with radioiodine. *J Nucl Med* 1994;35: 1418–1422.
11. Brincker H, Hansen HS, Andersen AP. Induction of leukaemia by ^{131}I treatment of thyroid carcinoma. *Br J Cancer* 1973;28:232–237.
12. Hall P, Holm LE, Lundell G, et al. Cancer risks in thyroid cancer patients. *Br J Cancer* 1991;64:159–163.
13. Sobels FH. Estimation of the genetic risk resulting from the treatment of women with ^{131}I. *Strahlentherapie* 1968;138:172–177.
14. Hayek A, Chapman EM, Crawford JD. Long-term results of treatment of thyrotoxicosis in children and adolescents with radioactive iodine. *N Engl J Med* 1970;283:949–953.
15. Winship T, Rosvoll RV. Thyroid carcinoma in childhood. Final report on a 20-yr study. *Proc Natl Cancer Conf* 1970;6:677–681.
16. Einhorn J, Hultén M, Lindsten J, Wicklund H, Zetterqvist P. Clinical and cytogenetic investigation in children of parents treated with radioiodine. *Acta Radiol* 1972;11:193–208.
17. Safa AM, Schumacher OP, Rodriguez-Antunez A. Long-term follow-up results in children and adolescents treated with radioactive iodine (^{131}I) for hyperthyroidism. *N Engl J Med* 1975;292:167–171.
18. Sarkar SD, Beierwaltes WH, Gill SP, Cowley BJ. Subsequent fertility and birth histories of children and adolescents treated with ^{131}I for thyroid cancer. *J Nucl Med* 1976;17:460–464.
19. Freitas JE, Swanson DP, Gross MD, Sisson JC. Iodine-131: optimal therapy for hyperthyroidism in children and adolescents? *J Nucl Med* 1979;20:847–850.
20. Halnan KE. Risks from radioiodine treatment of thyrotoxicosis. *BMJ* 1983;287:1821–1822.
21. Emrich D, Creutzig H. Benefits and risks of radioactive iodine therapy in differentiated thyroid carcinoma. *Prog Surg* 1988;19:133–146.
22. Casara D, Rubello D, Saladini G, et al. Pregnancy after high therapeutic doses of iodine-131 in differentiated thyroid cancer: potential risks and recommendations. *Eur J Nucl Med* 1993;20:192–194.
23. Dottorini ME, Lomuscio G, Mazzucchelli L, Vignati A, Colombo L. Assessment of female fertility and carcinogenesis after iodine-131 therapy for differentiated thyroid carcinoma. *J Nucl Med* 1995;36:21–27.
24. Schlumberger M, De Vathaire F, Ceccarelli C, et al. Exposure to radioactive iodine for scintigraphy or therapy does not preclude pregnancy in thyroid cancer patients. *J Nucl Med* 1996;37:606–612.
25. Izembart M, Chavaudra J, Aubert B, Vallée G. Retrospective evaluation of the dose received by the ovary after radioactive iodine therapy for thyroid cancer. *Eur J Nucl Med* 1992;19:243–247.
26. Schull WJ, Otake M, Neel JV. Genetic effects of the atomic bombs: a re-appraisal. *Science* 1981;213:1220–1227.
27. Otake M, Schull WJ, Neel JV. Congenital malformations, stillbirths and early mortality among the children of atomic bomb survivors: a re-analysis. *Radiat Res* 1990;122:1–11.
28. Sever LE, Gilbert ES, Hessol NA, McIntyre JM. A case-control study of congenital malformations and occupational exposure to low-level ionizing radiation. *Am J Epidemiol* 1988;127:226–242.
29. Tanaka K, Ohkura K. Evidence for genetic effects of radiation in offspring of radiological technicians. *Jpn J Hum Genet* 1958;3:135–145.
30. Li FP, Gimbrere K, Gelber RD, et al. Outcome of pregnancy in survivors of Wilms' tumor. *JAMA* 1987; 257:216–219.
31. Neel JV, Schull WJ, Awa AA, et al. The children of parents exposed to atomic bombs: estimates of the genetic doubling dose of radiation for humans. *Am J Hum Genet* 1990;46:1053–1072.
32. Gardner MJ, Snee MP, Hall AJ, et al. Results of case-control study of leukaemia and lymphoma among young people near Sellafield nuclear plant in West Cumbria. *Br Med J* 1990;300:423–429.
33. Sperling K, Pelz J, Wegner RD, Dörries A, Grüters A, Mikkelsen M. Significant increase in trisomy 21 in Berlin nine months after the Chernobyl reactor accident: temporal correlation or casual relation? *Br Med J* 1994;309:158–162.
34. Harjuletho T, Aro T, Rita H, Rytömaa T, Saxén L. The accident at Chernobyl and outcome of pregnancy in Finland. *Br Med J* 1989;288:995–997.
35. Bertollini R, Di Lallo D, Mastroiacovo P, Perucci CA. Reduction of births in Italy after the Chernobyl accident. *Scand J Work Environ Health* 1990;16:96–101.
36. Hawkins MM, Draper GJ, Winter DL. Cancer in the offspring of survivors of childhood leukemia and non-Hodgkin lymphomas. *Br J Cancer* 1995;71:1335–1339.
37. Auvinen A, Hakama M, Arvela H, et al. Fallout from Chernobyl and incidence of childhood leukemia in Finland, 1976–92. *Br Med J* 1994;309:151–154.
38. Hjalmars U, Kulldorf M, Gustafsson G. Risk of acute childhood leukaemia in Sweden after the Chernobyl reactor accident. *Br Med J* 1994;309:154–157.
39. Czeizel A. Hungarian surveillance of germinal mutations. Lack of detectable increase in indicator conditions caused by germinal mutations following the Chernobyl accident. *Hum Genet* 1989;82:359–366.
40. de Wals P, Bertrand F, de la Mata I, Lechat MF. Chromosomal anomalies and Chernobyl. *Int J Epidemiol* 1988;17:230–231.
41. Harjuletho-Mervaala T, Salnone R, Aro T, Saxén L. The accident at Chernobyl and trisomy 21 in Finland. *Mutat Res* 1992;275:81–86.
42. Boice J, Linet M. Chernobyl, childhood cancer and chromosome 21. Probably nothing to worry about. *Br Med J* 1994;309:139–140.
43. Holzman D. Will nuclear medicine survive outside the U.S.? *J Nucl Med* 1995;36:15N–43N.
44. Smith RA, Hawkins MM. Pregnancies after childhood cancer. *Br J Obstet Gynecol* 1989;96:378–380.
45. Simon R. Statistical methods for evaluating pregnancy outcomes in patients with Hodgkin's disease. *Cancer* 1980;45:2890–2892.
46. Origins of genetic disease [Editorial]. *Lancet* 1990; 335:887–888.

Investigations of Breast Tumors with Fluorine-18-Fluorodeoxyglucose and SPECT

Lutz-H. Holle, Ludwin Trampert, Sabine Lung-Kurt, Carlos E. Villena-Heinsen, Werner Püschel, Sylvia Schmidt and Erich Oberhausen

Departments of Nuclear Medicine, Gynecology and Pathology, University Clinics of Saarland, Homburg/Saar, Germany

Methods: We designed a prospective study to investigate the feasibility of combined FDG-SPECT and whole-body acquisition in the diagnostic work-up of breast tumors applying visual analysis. We studied 50 patients with breast tumors of unknown histology. **Results:** All malignant diseases were accurately detected in tumors >2.3 cm, while the smallest FDG-positive lesion was 1.4 cm. In a subgroup of these patients, quantitative evaluation (tumor-to-background ratios) was added, which improved the sensitivity. Lymph node metastases were accurately indicated in 9 of 13 patients, while the detection of distant metastases depended on the location and size. False-positive FDG scans were observed in inflamed tissue, in a rapidly growing phylloides tumor and in supposedly healthy breasts. **Conclusion:** These results are comparable with prior investigations of other groups using PET. Therefore, FDG-SPECT and whole-body acquisition may be an adequate and less expensive technique to meet the increasing demand of FDG examinations.

Key Words: fluorodeoxyglucose; breast tumors; SPECT; whole-body acquisition; radionuclide imaging

J Nucl Med 1996; 37:615–622

Received Feb. 23, 1995; revision accepted Jul. 30, 1995.

For correspondence or reprints contact: Lutz-H. Holle, MD, Department of Nuclear Medicine, University Clinics of Saarland, 66421 Homburg/Saar, Germany.

Breast cancer is one of the leading malignant diseases of women in the western hemisphere and is the most frequent cause of death from malignant disease in women (*1*). Prognosis depends on early detection of the primary tumor site and worsens after the development of metastases and disease progression (*2*). Standard imaging methods give accurate information in many patients, but there is concern that mammography results in many unnecessary surgeries to obtain needed histological information (*3*). Small lesions and recurrences after surgery often lead to diagnostic problems. Therefore, an imaging method to detect primary and metastatic malignancies and to distinguish between malignant and nonmalignant disease would be useful.

Recently, some efforts were made to use the glucose analog ^{18}F-fluoro-2-deoxy-D-glucose (FDG) for this purpose (*4,5*).

For several decades, tumor cells have been known to exhibit increased glycolytic activity due to a higher energy demand and changes in the intracellular enzymatic profile (*6,7*). FDG is phosphorylated like glucose by intracellular hexokinase and undergoes no further metabolism, a phenomenon which results in vigorous intracellular accumulation (*8,9*). Several experi-

mental tumors were investigated with FDG and all showed high FDG uptake suitable for PET or gamma camera imaging with specially fitted collimators (*9–13*). Human studies demonstrated the feasibility of FDG for imaging lymphomas (*14–16*), lung tumors (*17–19*), head and neck tumors (*20,21*), colon cancer (*22,23*), liver tumors (*24,25*), brain tumors (*26,27*), thyroid cancer (*28*) and breast cancer (*29,30*). FDG was used for primary and metastatic tumor detection and follow-up studies to assess the effectiveness of the tumor therapy (*5,25,31,32*). Thus, FDG is suitable for imaging tumors with enhanced glycolytic activity.

As a positron emitter, ^{18}F is best used with PET. PET centers are rare, however, and their limited access precludes PET studies for all patients with suspicious lesions. To reduce costs and improve investigational capacities, alternative techniques for imaging FDG (and other positron emitters) have become more common (*33–35*). Although the spatial resolution of gamma cameras is less than PET tomographs, their capacity for whole-body acquisition and its larger field of view are advantages. The purpose of this study was to investigate the usefulness of a commercially available dual-head gamma camera with specially designed high-energy collimators to evaluate breast tumors of unknown histology using a combination FDG-SPECT and whole-body technique.

MATERIALS AND METHODS

Patients

Fifty women (aged 20–82 yr, mean age 57 yr) suffering from breast tumors of unknown histology were studied. Each patient was told about the investigative nature of the study and its potential risks and benefits before informed consent was obtained prior to the investigation. The studies were performed between March 1993 and May 1994. All tumors were identified by mammography and/or ultrasound before the examination. Histology was confirmed by surgery or biopsy within 14 days after the investigation. The number of investigations was limited by the restricted availability of the FDG, with the possibility of up to four investigations per week.

Gamma Camera

Images were obtained on a commercially available dual-head gamma camera with two rectangular (50.8 × 35.6 cm) NaI(Tl) crystals. Crystal thickness was 0.5 in for better detection efficiency of the annihilation photons. The intrinsic efficiency for 500 keV photons relative to those at 70 keV (100%) is 36% for the 0.5 in crystal compared to 28% for a 0.375 in crystal, respectively, according to information of the manufacturer. Thus, compared to a 0.375 in crystal, the detection efficiency for 511 keV photons is increased by 29.5% using 0.5 in crystals. The photomultiplier tubes and the preamplifiers are analog, starting at the summing circuitry the camera operates digitally. The analyzer electronics were adjusted by the manufacturer to accommodate 511 keV photons. The camera was shielded accordingly and with extra-high energy collimators (hexagonal hole diameter 6.6 mm, septa thickness 3.3 mm, septa length 90 mm). The calculated septal penetration was 12% using a Gaussian fit of the line spread function (*36*). The sensitivity maps were created with a planar phantom with ^{18}F in water, collecting 120×10^6 counts per head. The system sensitivity with the extra high-energy collimators was measured to 66 cpm/37 MBq for ^{18}F (for ^{99m}Tc, it was 163 cpm/37 MBq). The system resolution was 1.4 cm FWHW at a 10-cm distance from the collimator surface in water (*37*).

Imaging Procedure

Patients received 500–1000 MBq FDG as a bolus injection after fasting overnight. Thus, the majority of the patients showed little or no myocardial physiological FDG uptake, resulting in improved imaging conditions for the detection of tumorous tissue, i.e., breast lesions. FDG was produced by the Kernforschungszentrum Karlsruhe and transported to our department by courier service over a distance of 100 km. Fluorine-18 was produced by the ^{18}O (p, n)^{18}F nuclear reaction using highly enriched ^{18}O water. The reaction in an IBA processing module is based on the transfer mediated substitution of triflate by [^{18}F]fluoride. The nonpyrogenic FDG solution had a radiochemical purity higher than 95%.

Anterior and posterior whole-body acquisition started 50 min after the FDG application using a scan speed of 15 cm/min. During the whole-body acquisition, patients were in the supine position. The subsequent SPECT acquisition was performed in the prone position to increase the breast's distance from the chest. Sixty views were acquired over 360°, and 5–6 × 10^6 counts were collected per study. Acquisition of 360° SPECT images ensured that the breast lesions, axillary lymph nodes and distant metastases could be detected with adequate quality. Attenuation artifacts using 360° SPECT images (instead of 180°) are unlikely, since high-energy photons undergo little absorption in tissue. If whole-body scan demonstrated suspicious FDG accumulation outside the thorax region, additional SPECT scans were acquired when possible.

Data were saved in a 64-word mode matrix for further analysis. A Butterworth filter with a cutoff of 0.7 and order 5 was used for data reconstruction. No attenuation correction was performed. Color images of three planes were printed for the interpretation. In some difficult cases, the volume-rendered images and the cine mode were helpful tools in the interpretation procedure. Image review and interpretation were performed by two experienced clinicians blinded to the results from other imaging studies. FDG accumulation in the tumors was scored visually as four grades: from 0 = no accumulation, to 3 = high accumulation. This grading actually represented the visual tumor-to-background ratios. Grades 2–3 were regarded as abnormal increased for the primary tumors (*29*), and for the lymph nodes, any increase in accumulation was interpreted as pathologic (grade 1–3).

In most patients, quantitative retrospective analysis of the lesions could be performed. Regions of interest (ROIs) were defined for the primary lesion, the opposite breast and for normal breast tissue (background), which often correlates with the opposite breast. Ratios of the mean count rate of the lesions' ROI versus background were calculated. Due to the retrospective character, these ratios were not used for further evaluation of the results.

The results were compared to those of the other imaging techniques (ultrasound, mammography, ^{99m}Tc-MDP bone scan, radiography and MRI). Histological results were considered the gold standard for further evaluation. The tumor size was measured histologically. If this was not possible, the largest diameter of other imaging methods was used if lesion could be accurately differentiated from surrounding tissues.

RESULTS

Nineteen of 23 histologically benign primary lesions showed little or no FDG uptake corresponding to low-grade visual uptake (score 0–1). All results are summarized in Table 1. One patient with a rapidly growing phylloides tumor, one with fibrocystic mastopathy of both breasts, one with acute suppurative mastitis (Fig. 1) and one with chronic inflammation had high FDG uptake. The ratios for the acute suppurative mastitis and for the fibrocystic mastopathy were significantly increased (>1.6, Table 1). All other ratios of benign lesions and healthy breasts without indication for malignancy had values <1.6.

Eighteen of the 27 patients with primary malignant diseases exhibited high-grade visual uptake scores (Fig. 2). The sizes ranged from 1.4 cm (Fig. 3) to 10 cm (mean ± s.d. 3.62 ± 0.4

TABLE 1
Clinical Results (Primary Lesions)

Patient no.	Age (yr)	Histology	Tumor size (cm)	TNM (UICC)	Uptake grade	Evaluation	Location	L/Bckg	R/Bckg
1	78	Ductal carcinoma	0.7	pT1 pN0, G2	0	FN	L	1.88	0.92
2	73	Ductal carcinoma	1.3	pT1 pN0	0	FN	L	2.08	1.32
3	72	Ductal carcinoma	1.2	pT1 pN0, G2	0	FN	R	0.99	1.01
4	69	Ductal carcinoma	1.4	pT1c pN0, G2	1	FN	R	1.25	1.56
5	62	Ductal carcinoma	1.7	pT1 pN0, G2	0	FN	R	0.98	2.20
6	80	Comedo carcinoma	1.8	pT1 pN0	0	FN	R	1.21	1.51
7	73	Ductal carcinoma	<2	pT1b pN0, G2	0	FN	L	1.86	1.37
8	71	Comedo carcinoma in situ	2	pTis	0	FN			
9	47	Lobular carcinoma	2.3	pT2 pN1b	1	FN	L,R*	1.71	1.96
10	77	Ductal carcinoma	1.4	pT2 pN0, G2	2	RP	L	1.65	0.88
11	65	Ductal carcinoma	1.5	pT2 pN0, G3	3	RP			
12	80	Ductal carcinoma	1.5	pT2 pN1, G3	2	RP			
13	64	Ductal carcinoma	1.8	pT1c pN1	2	RP			
14	82	Ductal/lobular carcinoma	2.1	pT2 pN0, G2	3	RP	R	0.35	2.23
15	51	Ductal carcinoma	2.3	pT2 pN0, G3	3	RP	R	0.98	5.29
16	65	Ductal carcinoma	2.4	pT2 pN2, G3	3	RP			
17	64	Ductal carcinoma	2.5	pT2 pN1	3	RP			
18	68	Ductal carcinoma	2.8	pT2 pN1, G2	3	RP	L	9.24	1.00
19	49	Comedo carcinoma	3	pT2 pN0, G2	2	RP	R	1.10	3.52
20	63	Ductal carcinoma	3.5	pT2 pN0, G2	3	RP	R	0.95	6.22
21	69	Ductal carcinoma	4.2	pT4 pN2, G3	3	RP			
22	43	Ductal carcinoma	5	pT3 pN1, G2	3	RP			
23	72	Ductal carcinoma	5	pT4 pN1	3	RP	L	3.53	0.90
24	53	Ductal carcinoma	6	pT3 pN2, G3	3	RP			
25	72	Ductal carcinoma	6.5	pT4 pN1, G2	3	RP			
26	46	Ductal carcinoma	10	pT4 pN2 pM1 (ovar, liver), G3	3	RP	L	7.16	0.73
27	77	Ductal carcinoma	NA	pTis	2	RP	L	2.10	0.84
28	55	Chronic inflammation	1.5		2	FP			
29	45	Fibrocystic mastopathy	1.8		2	FP	L,R	2.10	2.03
30	48	Acute supparative mastitis	2.7		3	FP	R	0.93	4.35
31	55	Phylloides tumor	6		3	FP			
32	59	Fibrous mastopathy	NA		0	RN	L,R	1.51	1.58
33	69	Fibrocystic mastopathy	NA		0	RN	L,R	1.02	1.07
34	48	Fibrocystic mastopathy	NA		1	RN	L,R	1.39	1.24
35	49	Fibrous mastopathy	NA		0	RN			
36	52	Fibrocystic mastopathy	NA		0	RN			
37	80	Atrophic mammarian tissue	0.8		0	RN	L	1.14	1.48
38	34	Fibrocystic mastopathy	1		1	RN	L,R	1.00	1.25
39	21	Normal tissue	1.5		0	RN	R	1.27	1.40
40	37	Fibroadenoma	1.6		0	RN	R	1.42	1.53
41	23	Fibrous mastopathy	1.6		0	RN	R	0.93	0.98
42	19	Fibroadenoma	1.8		0	RN			
43	38	Fibroadenoma	1.8		0	RN	R	1.31	1.28
44	40	Fibrocystic mastopathy	2		1	RN	L	1.31	1.17
45	44	Fibrous mastopathy	2		1	RN			
46	54	Fibrocystic mastopathy and chronic inflammation	2		1	RN	L	1.35	1.22
47	25	Fibroadenoma	2.9		1	RN	L	1.43	1.34
48	52	Fibroadenoma	>2		1	RN			
49	53	Normal tissue	4		0	RN	L,R	1.44	0.96
50	65	Chronic infammation	4		0	RN	L	1.32	0.52

*Follow-up proved malignancies of both breasts as indicated by the quantitative data.

FN = false-negative; TP = true-positive; FP = false-positive; TN = true-negative; NA = not available; L,R = lesion in the left, right breast; L/Bckg and R/Bckg are calculated tumor-to-background ratios (due to techniqual reasons not always available).

cm), whereas false-negative tumors were significantly smaller: with 0.7–2.3 cm in diameter (mean ± s.d. 1.55 ± 0.5). By using the ratios, five additional malignant tumors could be accurately identified with values >1.6. The smallest had an extension of only 0.7 cm in diameter (Table 1), but three tumors of 1.2, 1.4, and 1.8 cm still showed no significant FDG uptake.

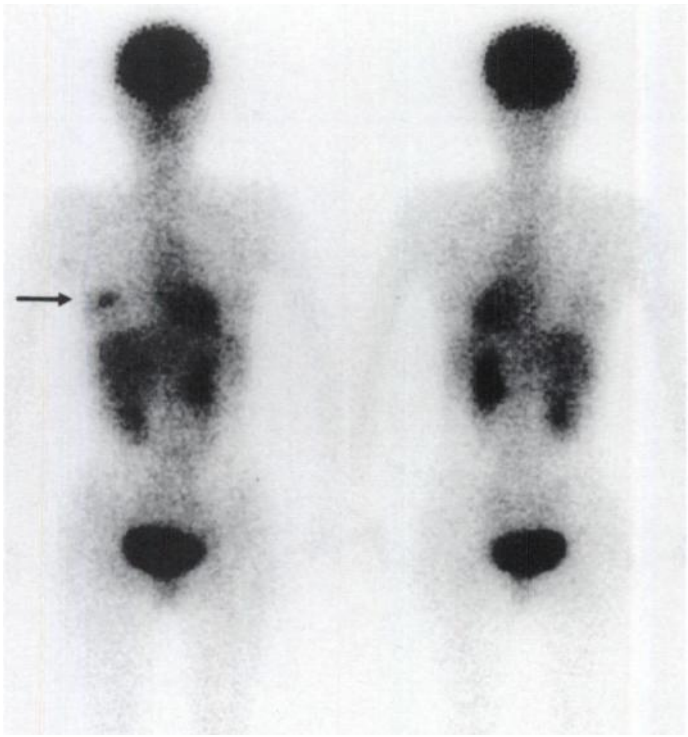

FIGURE 1. Patient suffering from acute suppurative mastitis (arrow). Anterior and posterior planar whole-body scans from 50 min after injection of 500 MBq [^{18}F]FDG demonstrate high focal uptake. Physiological uptake into brain, liver, heart and due to excretion kidneys and bladder (Patient 30, Table 1).

In addition, 9 of 12 axillary lymph node metastases were visualized exhibiting increased metabolic activity. All false-negative lymph node metastases were smaller than 0.8 cm in diameter. The positive lymph nodes were at least 1.7 cm in the longest diameter. Patients with metastatic disease are listed in Table 2.

Distant metastases were defined by other imaging techniques in three patients. Liver metastases showed high FDG uptake in the planar whole-body scan in two patients. In one patient, a single lesion 3 cm in diameter was clearly detected by focal FDG uptake. The other patient demonstrated two focal lesions on the whole-body scan, while ultrasound suggested multiple foci within the whole liver. Therefore, at least two of these metastases exhibited high glycolytic activity.

In three patients, bone metastases were evident on the ^{99m}Tc-MPD bone scan. In these three patients, FDG whole-body scans showed at least one skeletal focus. One single metastasis of the massa lateralis showed high uptake of both FDG and MPD. In one patient, the MPD bone scan demonstrated multiple metastases of the whole spinal column, the pelvis and the right humerus, while the FDG whole-body scan demonstrated focal uptake only in the right humerus, pelvis and lumbar spine. Radiographic investigation, however, showed osteolysis in only those metastases that were detected by FDG (Fig. 4). The MPD scan of the third patient demonstrated only slightly enhanced osteoblastic activity, while the FDG scan and SPECT scans demonstrated malignant bone infiltration of large parts of the spine and pelvis, even in areas without osteolysis proven radiographically.

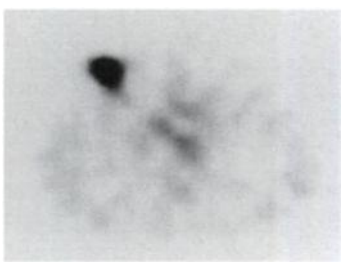

FIGURE 2. Transverse slice of a ductal carcinoma of the right breast with a maximum diameter of 2.3 cm. High focal uptake 60 min after injection of 550 MBq [^{18}F]FDG (Patient 15, Table 1).

FIGURE 3. Sagittal slice of a ductal carcinoma of the left breast (arrow) with a maximum diameter of 1.4 cm. Increased focal uptake in front of the heart 60 min after injection of 450 MBq ^{18}F-FDG (Patient 10, Table 1).

Detection of one lung metastasis (2 cm) behind the heart and one ovarian metastasis was unsuccessful, probably due to the adjacent heart and bladder which exhibit physiologically high FDG uptake. Reduced uptake of the cancer bearing breast compared with the healthy breast was observed in one patient. There was no indication of inflammation or benign alterations of the healthy breast by other imaging techniques. Further follow-up of this patient (Patient 9, Table 1), however, demonstrated malignant disease in the opposite breast 4 mo later. Both sides demonstrated ratios >1.6. Therefore, malignant disease of both breasts was retrospectively indicated by FDG-SPECT only.

One other patient had unsuspicious mammography results, ultrasound and clinical examination, but sanguinous secretion of the mamma. Again, only FDG-SPECT images demonstrated pathologically increased FDG uptake, and a small ductal carcinoma (pTis) was proved histologically (Patient 27).

DISCUSSION

General Considerations

Due to its favorable accumulation characteristics, FDG has become an important radiopharmaceutical in nuclear medicine and oncology. It has been used for the detection and follow-up of primary and metastatic disease of different malignant tumors. These studies revealed high sensitivity for the detection of malignant disease, but there are no data on the specificity of FDG uptake for malignant disease with FDG as a marker for glycolytic activity.

FDG studies are almost exclusively performed with PET scanners. Due to the limited availability and the high operating costs of PET, alternative techniques for the detection of the annihilation photons are of increasing interest. Although multicrystal gamma cameras (*33*), multiwire detectors and seven pinhole SPECT (*34*) did not gain wide recognition, specially collimated conventional gamma cameras (*35*) have become more accepted in clinical use. Low cost and high availability are two important advantages of FDG-SPECT. Also, the large field of view and the possibility for whole-body acquisition are other advantages in oncologic imaging.

TABLE 2
Patients with Metastatic Disease

Patient no.	Age (yr)	Histology	Metastases	Evaluation
9	47	Lobular carcinoma	Follow-up proved malignancy of opposite breast	TP
			LN (<0.8 cm)	FN
12	80	Ductal carcinoma	LN axilla (<0.5 cm)	FN
13	64	Ductal carcinoma	LN axilla	FN
16	65	Ductal carcinoma	LN axilla (1.7 cm)	TP
			LN axilla (0.8 cm)	TP
17	64	Ductal carcinoma	LN axilla (2 cm)	TP
18	68	Ductal carcinoma	LN axilla	FN
20	63	Ductal carcinoma	Left massa lateralis bone DPD-positive metastasis (normal radiograph)	TP
21	69	Ductal carcinoma	LN axilla (3.5 cm)	TP
22	43	Ductal carcinoma	LN axilla (<0.8 cm)	FN
23	72	Ductal carcinoma	2 LN axilla	2 × TP
24	53	Ductal carcinoma	LN axilla (2 cm)	TP
			Liver (3 cm)	TP
			Lung (2 cm, adjacent to heart)	FN
			Multiple bone metastases:	
			(a) osteolytic by radiograph	TP
			(b) normal radiograph	FN
25	72	Ductal carcinoma	LN axilla (<2 cm)	TP
26	46	Ductal carcinoma	2 LN axilla	2 × TP
			Multiple liver metastases	2 × TP
			Multiple bone metastases	TP
			Ovaries	FN

FN = false negative, TP = true positive, FP = false positive, LN = lymph node.

Primary Tumor Detection

All malignant tumors with an extension >2.3 cm were identified by increased FDG uptake. In addition, 6 of 15 tumors below this size were accurately characterized as malignant. Five additional tumors could be identified accurately as malignant by retrospective quantitative evaluation. The smallest had a diameter of only 0.7 cm, which is below the system's resolution. This exemplifies that the target-to-nontarget contrast ratio is more important for the detectability than system resolution.

On the other hand, one 2.3-cm lesion and seven 2-cm or less lesions showed no significantly increased FDG uptake. Minn and Soini investigated 17 patients with planar gamma camera technique and had 18% false-negative FDG scans (*29*). Compared to their results, we had a considerably higher number of false-negative FDG scans (33%). One must consider, however, that seven of the nine patients with false-negative results had stage pT1 (by UICC) tumors (i.e., small tumors), whereas Minn and Soini only had 1 of 17 patients with a tumor in this stage. Therefore, any differences should be attributed to variances in patient population (i.e., tumor sizes). Based on our quantitative analysis, we had a false-negative rate of 14% (at a threshold of 1.6). In the Wahl et al. (*30*) study, FDG-PET accurately (attenuation-corrected images) detected breast tumors of at least 3.2-cm in diameter in ten patients with no false-negative scans. Larger tumors obviously are not problematic in conventional diagnostic procedures; tumors 3.2 cm or larger were accurately detected in our study as well. Hoh et al. (*5*) used whole-body PET techniques (*38*) in breast cancer studies and could detect tumors with a minimum extension of 1 cm compared to 1.4 cm in our FDG-SPECT study. Tumor size, however, should not be the limiting factor. If the radionuclide uptake is high enough, the hot spot imaged indicates the presence of disease but does not provide data on geometric size. Therefore, even a point accumulation would be detected if the resulting average count rate within one voxel leads to sufficient contrast. Theoretically, a reduction in pixel size would contribute to increased ratios, but it is not useful since the spatial resolution is already lower than the pixel size, (i.e., the difference between pixel (voxel) size and the resolution elements).

Lymph Node Involvement

Lymph node metastases were accurately detected in 9 of 13 patients in our study. Of course, spatial resolution did not allow discrimination of each involved lymph node, but increased FDG uptake (due to several involved lymph nodes in some patients) accurately indicated metastatic disease. In general, the limited spatial resolution of any imaging device will not allow for precise delineation of adjacent lymph nodes presenting FDG uptake. Therefore, a difference in the number of surgical specimens and imaging results is to be expected. In contrast to primary tumors, lymph node metastases are in an environment of physiologically higher FDG uptake. Since muscle and liver represent the primary form of glucose (and FDG) storage after glucose administration (*39*), dietary conditions do influence its glucose and FDG uptake markedly (*40*). Malignant cells, on the other hand, supposedly have maximum glycolytic activity already (*7*). Higher glucose levels lead to a higher competition at the transporter proteins and, consequently, to impaired FDG uptake into the malignant cells, although no influence from insulin was observed (*13,41*).

Dietary Considerations

Fasting results in low glucose, low insulin and relatively higher FDG blood levels and, due to reduced utilization rates, in enhanced plasma half-life times. The best target-to-background ratio for distant metastases of breast cancer should be obtained after fasting. The duration of fasting is debatable (*4*). Yamada

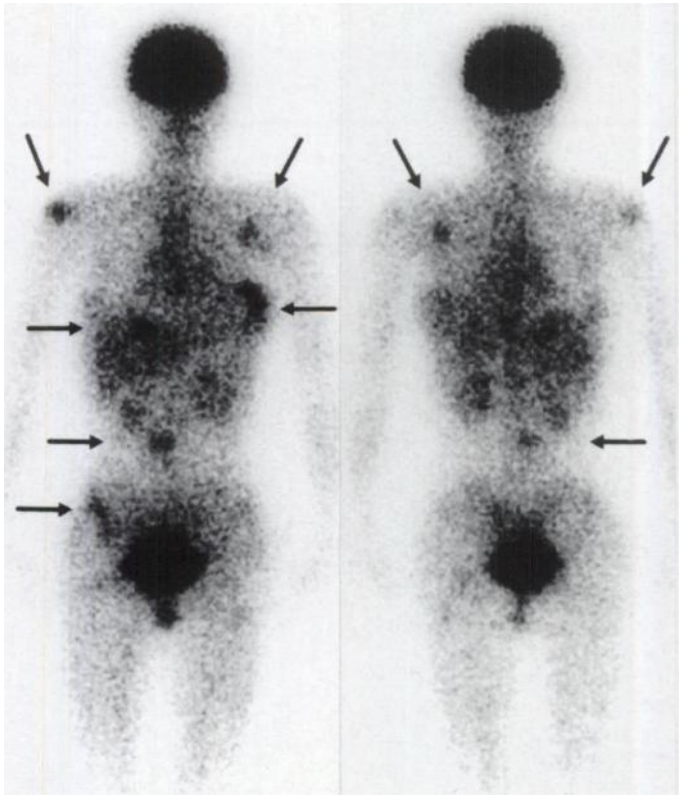

FIGURE 4. Ductal carcinoma of the left breast with multiple metastases 50 min after injection of 450 MBq ^{18}F-FDG. Anterior (left) and posterior (right) planar whole-body scans demonstrate multiple FDG uptake in the primary lesion and metastases (arrows). All above bone foci demonstrated osteodestruction in the radiograph; additional bone metastases were found in the MDP bone scan (Patient 24, Tables 1, 2).

et al. (*42*) described remarkably decreased myocardial FDG uptake in rats after 12 hr and even less after 24 hr of fasting. After this period, no further decrease was observed. Berry et al. (*43*), however, found good myocardial PET image quality in 50% of patients after 12 hr of fasting (*43*). Therefore, in some patients, myocardial (and muscular) FDG uptake was evident in the whole-body scan even after 12 hr of fasting. Thus, all increased focal FDG uptake in the axillary region was judged as pathologic.

A principal problem in detecting primary and metastatic disease is variances in FDG accumulation. Joensuu and Ahonen (*28*) observed thyroid carcinoma metastases with and without ^{131}I and with and without FDG accumulation in the same patients, and did not find any correlation between the different uptake behaviors. There may even be different accumulation characteristics between the primary tumor and its metastases leading to higher FDG uptake to axillary lymph node metastases than in breast carcinoma (*30*). The heterogeneity of the primary tumor, as well as the metastases, is exhibited in a wide range of biological characteristics, including enzymes, growth properties, sensitivities to various therapeutic agents, etc. (*44*).

Distant Metastases

A solitary liver metastasis demonstrated increased focal uptake, but in one other woman only two foci were detected, while ultrasound indicated multiple liver metastases. Physiologically high FDG uptake of the liver cells (plasma glucose regulation) follows high FDG clearance due to high glucose-6-phosphate activity (*7*) of the liver cells. The subsequent demarcation of the malignant tissue allows the detection of metastases and primary liver tumors as firstly described by Paul et al. (*24*).

Bone metastases were detected in three cases and were found to be lower, higher and identical in sensitivity compared to the MDP bone scans. In one patient, only osteolytic metastases (confirmed by x-ray) were detected by the FDG whole-body scan, while the MDP bone scan showed metastases of the whole spinal column. Another patient had only slightly increased osteoblastic activity with increased glycolytic activity. A follow-up bone scan 3 mo later demonstrated increased osteoblastic activity in the regions of increased FDG uptake measured 3 mo earlier. The third patient had only one bone metastasis detected by both FDG and MDP. Previously, MDP-negative bone metastases of myeloma and esophageal carcinoma had been detected with high FDG uptake (*45*). Minn and Soini reported an MDP-negative bone metastasis in breast cancer with high FDG uptake while an osteoporotic fracture showed inverse accumulation characteristics (*29*). Comparison with radiographs demonstrated no clear correlation of osteolysis and FDG uptake in our patients.

FDG-SPECT did not detect distant metastases in two patients: one lung metastasis behind the heart and an ovarian metastasis close to the bladder. Supposedly due to physiologically increased FDG uptake of the adjacent heart, a 2-cm lung metastasis was not detected due to low target-to-background ratios and limited spatial resolution. The ovarian metastasis was not seen on the planar study and SPECT was not performed in this region. The metastasis might have been seen in SPECT reconstructions.

In one patient (Patient 9), the supposedly healthy breast demonstrated higher FDG uptake than the breast with cancer which was interpreted as a false-negative result. Further follow-up of this patient proved advanced cancer on the supposedly healthy breast 4 mo later. The lower uptake compared to the opposite breast lead to a false low uptake grading of the cancer-bearing breast but, as retrospectively estimated, the ratios indicated malignancies in both breasts. In fact, the other imaging methods, except FDG-SPECT, did not detect metastases in the "healthy" breast.

In Patient 27, negative results of the other imaging methods, except FDG-SPECT, led to normal diagnosis, but malignant disease was proven histologically.

Since FDG is a glucose analog, it is not surprising that nonmalignant diseases also accumulate FDG when they have increased glycolytic activity. Hoh et al. (*5*) also found FDG uptake in benign mammarian fibroadenomas. Our observations demonstrated little or no FDG uptake in most of the fibroadenomas. Only one fibrocystic mastopathy showed significant FDG uptake and increased target-to-background ratios in both breasts (Patient 29). High-grade FDG uptake was also observed in one phylloides tumor which grew to 6 cm in diameter within 7 wk. Thus, increased metabolic activity is obvious but, for lesion histology, had to be evaluated as false-positive.

Inflammation

In two patients with increased FDG uptake, acute and chronic inflammation could be proven histologically. High FDG uptake was observed in both abdominal and cerebral abscesses in human PET studies (*46,47*), while sterile turpentine abscesses did not accumulate FDG in rabbits (*9*). Examinations of the intratumoral distribution of FDG demonstrated high uptake into

macrophages and granulation tissue and significantly less FDG uptake in the tumor cells themselves (*48*). About 30% of the tumor mass may be due to macrophage infiltration (*49*). These results suggest that FDG uptake of tumors with high macrophage content is due to these cells rather than to the tumor cells themselves. On the other hand, follow-up studies demonstrated a correlation between FDG uptake and the aggressiveness of different malignant diseases (*15,20*), suggesting that the proliferation rate determines the FDG uptake in cancer cells. This observation is suggested by a correlation between S-phase cells measured by DNA flow cytometry and the FDG uptake in both planar and PET studies (*20,21*). Follow-up studies, however, have to consider the macrophage content and the presence of granulation tissue in the tumor.

The lower detection sensitivity of the gamma camera for the 511-keV photons made it necessary to apply an activity which was higher than usual for PET investigations. This caused higher radiation doses for the patient and the nuclear staff. The latter could be reduced by sufficient additional shielding during the investigation. The former was, in our view, tolerable since the method offers the possibility to investigate both primary and metastatic disease. Theoretically, it may be a problem in patients with benign lesions, but the radiation dose should play a minor role in view of the diagnostic value.

Alternative Methods

A direct comparison of our results with FDG-PET would have been desirable to determine if possible differences were of clinical relevance. The dynamic character of the FDG distribution could be problematic since the time of investigation after the application may influence the results. Therefore, a two-day protocol would be necessary for comparative purposes, resulting in reduced acceptance by the women on one hand and to further radiation exposure on the other.

We will compare our FDG-SPECT results with ^{99m}Tc-methoxyisobutylisonitrile (MIBI) in future studies since other groups have obtained excellent results with MIBI in the evaluation of breast tumors (*50,51*). Even if the data for primary lesions are encouraging, we see problems with the detection of lymph node and metastatic disease. The high muscular uptake and excretion through the liver suggest increased background activity when using MIBI. In addition, the muscular uptake cannot be influenced by fasting in contrast to FDG.

MRI in combination with dynamic gadolinium-DTPA studies gives accurate information in primary breast tumors (*52,53*), but it requires correct lesion measurement, which may be difficult in advanced mastopathy. In addition, simultaneous evaluation of lymph nodes and distant metastases is not possible with one investigation. Therefore, FDG as a marker for glycolytic activity offers some advantages compared to MIBI and dynamic MRI for breast tumor imaging.

CONCLUSION

Combined whole-body FDG scans and FDG-SPECT with a dual-head gamma camera offers an attractive and practical alternative to FDG-PET investigations. The technique is feasible for imaging primary and metastatic breast cancer and, because FDG uptake is indicative of metabolism, it provides additional data in unclear cases. Low FDG uptake in tumors larger than 2–2.5 cm is not indicative of malignancy. The lower spatial resolution of SPECT may be of minor importance if the FDG uptake is high even in small lesions. Quantitative evaluation of tumor-to-background ratios improves the accuracy and should be performed routinely. Recently, a technique for whole-body PET was introduced (*38*), but it is not readily available. Therefore, the combined FDG-SPECT and whole-body technique with a specially equipped gamma camera may be a temporary solution to the increasing demand for FDG tumor investigations.

REFERENCES

1. American Cancer Society. *Cancer figures and facts*. New York: American Cancer Society; 1990.
2. Jotty GS. New prognostic indicators in resectable breast cancer. *Anticancer Res* 1991;9:1227–1232.
3. Gisvold. Imaging of the breast: techniques and results. *Mayo Clin Proc* 1990;65:56–66.
4. Hawkins RA, Choi Y, Huang S-C, et al. Quantitating tumor glucose metabolism with FDG and PET. *J Nucl Med* 1992;33:339–344.
5. Hoh CK, Hawkins RA, Glaspy JA, et al. Cancer detection with whole-body PET using 2-[^{18}F]fluoro-2-deoxy-D-glucose. *J Comput Assist Tomogr* 1993;17:582–589.
6. Warburg O. On the origin of cancer cells. *Science* 1956;123:309–314.
7. Weber G. Enzymology of cancer cells. *N Engl J Med* 1977;296:541–551.
8. Gallagher BM, Fowler JS, Gutterson NI, et al. Metabolic trapping as a principle of radiopharmaceutical design: some factors responsible for the biodistribution of [^{18}F]2-deoxy-2-fluoro-D-glucose. *J Nucl Med* 1978;19:1154–1161.
9. Som P, Atkins HL, Bandoypadhyay D, et al. A fluorinated glucose analog, [^{18}F]2-fluoro-2-deoxy-D-glucose: nontoxic tracer for rapid tumor detection. *J Nucl Med* 1980;21:670–675.
10. Larson SM, Weiden PL, Grunbaum Z, et al. Positron imaging studies. II. Characteristics of 2-deoxyglucose uptake in rodent and canine neoplasms: concise communication. *J Nucl Med* 1981;22:875–879.
11. Paul R, Johansson R, Kellokumpu-Lehtinen P-L, Söderström K-O, Kangas L. Tumor localization with ^{18}F-2-fluoro-2-deoxy-D-gucose: comparative autoradiography, glucose-6-phosphatase histochemistry and histology of renally implanted sarcoma of the rat. *Res Exp Med* 1985;185:87–94.
12. Wahl RL, Hutchins GD, Buchsbaum DJ, et al. Fluorine-18-2-deoxy-2-fluoro-D-glucose uptake into human tumor xenografts. *Cancer* 1991;67:1544–1550.
13. Wahl RL, Henry CA, Ethier SP. Serum glucose: effects on tumor and normal tissue accumulation of 2-[^{18}F]-fluoro-2-deoxy-D-glucose in rodents with mammary carcinoma. *Radiology* 1992;183:643–647.
14. Paul R. Comparison of fluorine-18-2-fluorodeoxyglucose and gallium-67-citrate imaging for detection of lymphoma. *J Nucl Med* 1987;28:288–292.
15. Rosenfeld SS, Hoffman JM, Coleman RE, et al. Studies of primary central nervous system lymphoma with fluorine-18-fluorodeoxyglucose positron emission tomography. *J Nucl Med* 1992;33:532–536.
16. Okada J, Yoshikawa K, Imazeki K, et al. The use of FDG-PET in the detection and management of malignant lymphoma: correlation of uptake with prognosis. *J Nucl Med* 1991;32:686–691.
17. Gupta NC, Frank AR, Dewan NA, et al. Solitary pulmonary nodules: detection of malignancy with PET with 2-[^{18}F]-fluoro-2-deoxy-D-glucose. *Radiology* 1992;184:441–444.
18. Kubota K, Matsuzawa T, Fujiwara T, et al. Differential diagnosis of lung tumor with positron emission tomography: a prospective study. *J Nucl Med* 1990;31:1927–1933.
19. Nolop KB, Rhodes CG, Brudin LH, et al. Glucose utilization in vivo by human pulmonary neoplasms. *Cancer* 1987;60:2682–2689.
20. Minn H, Joensuu H, Ahonen A, Klemi P. Fluorodeoxyglucose imaging: a method to assess the proliferative activity of human cancer in vivo. *Cancer* 1988;61:1776–1781.
21. Haberkorn U, Strauss LG, Reisser C, et al. Glucose uptake, perfusion and cell proliferation in head and neck tumors: relation of positron emission tomography to flow cytometry. *J Nucl Med* 1991;32:1548–1555.
22. Yonekura Y, Benua RS, Brill AB, et al. Increased accumulation of 2-deoxy-2-[^{18}F]fluoro-D-glucose in liver metastases from colon carcinoma. *J Nucl Med* 1982;23:1133–1137.
23. Haberkorn U, Strauss LG, Dimitrakopoulou A, et al. PET studies of fluorodeoxyglucose metabolism in patients with recurrent colorectal tumors receiving radiotherapy. *J Nucl Med* 1991;32:1485–1490.
24. Paul R, Ahonen A, Roeda D, Nordman E. Imaging of hepatoma with ^{18}F-fluorodeoxyglucose [letter]. *Lancet* 1985;1:50–51.
25. Okazumi S, Isono K, Enomoto, et al. Evaluation of liver tumors using fluorine-18-fluorodeoxyglucose PET: characterization of tumor and assessment of effect of treatment. *J Nucl Med* 1992;33:333–339.
26. DiChiro G, Hatazawa J, Katz DA, Rizzoli HV, DeMichele DJ. Glucose utilization by intracranial meningeomas as an index of tumor agressivity and probability of recurrence: a PET study. *Radiology* 1987; 164:521–526.
27. Tyler JL, Diksic M, Villemure J-G, et al. Metabolic and hemodynamic evaluation of gliomas using positron emission tomography. *J Nucl Med* 1987;28:1123–1133.
28. Joensuu H, Ahonen A. Imaging of metastases of thyroid carcinoma with fluorine-18-fluorodeoxyglucose. *J Nucl Med* 1987;28:910–914.
29. Minn H, Soini I. Fluorine-18-fluorodeoxyglucose scintigraphy in diagnosis and follow up of treatment in advanced breast cancer. *Eur J Nucl Med* 1989;15:61–66.
30. Wahl RL, Cody RL, Hutchins GD, Mudget EE. Primary and metastatic breast carcinoma: initial clinical evaluation with PET with the radiolabeled glucose analogue 2-[^{18}F]-fluoro-2-deoxy-D-glucose. *Radiology* 1991;179:765–770.
31. Ichiya Y, Kuwabara Y, Otsuka M, et al. Assessment of response to cancer therapy using fluorine-18-fluorodeoxyglucose and positron emission tomography. *J Nucl Med* 1991;32:1655–1660.
32. Wahl R, Zasadny K, Helvie M, et al. Metabolic monitoring of breast cancer chemohormonotherapy using positron emission tomography: initial evaluation. *J Clin Oncol* 1993;11:2101–2111.
33. Cochavi S, Goldsmith SJ, Strashun A, Nadelman J. Planar imaging of positron emitting radionuclides with a multicrystal camera. *J Nucl Med* 1982;23:722–730.
34. Höflin F, Ledermann H, Noelpp U, Weinreich R, Roesler H. Routine ^{18}F-2-deoxy-2-

fluoro-D-glucose myocardial tomography using a normal large field of view gamma camera. *Angiology* 1989;40:1058–1064.
35. vanLingen A, Huijgens PC, Visser FC, et al. Performance characteristics of a 511-keV collimator for imaging positron emitters with standard gamma camera. *Eur J Nucl Med* 1992;19:315–321.
36. Schaefer A, Oberhausen E. Physical performance of a multispect–two gamma camera for imaging positron emitters. (Testmessungen an der Multispect-2-Gammakamera zum Nachweis von 511 keV-gammastrahlung). *Nuklearmedizin* 1995;34:40–46.
37. NEMA Standards Publication No. NU 1: Performance characteristics of scintillation cameras. 1986.
38. Dahlbom M, Hoffman EJ, Hoh CK, et al. Whole-body positron emission tomography. Part I. Methods and performance characteristics. *J Nucl Med* 1992;33:1191–1199.
39. Björntorp P, Sjoström L. Carbohydrate storage in man. Speculations of some quantitative considerations. *Metabolism* 1978;27(suppl 2):1853–1863.
40. Thiebaud D, Jacot E, DeFronzo RA, et al. The effect of graded doses of insulin on total glucose uptake, glucose oxidation and glucose storage in man. *Diabetes* 1982;31:957–963.
41. Wahl RL, Henry C, Ethier S. Serum glucose effects on the tumor and normal tissue uptake of FDG in rodents with breast carcinoma [Abstract]. *J Nucl Med* 1990;31:888–889.
42. Yamada K, Endo S, Fukuda H, et al. Experimental studies on myocardial glucose metabolism of rats with ^{18}F-2-fluoro-2-deoxy-D-glucose. *Eur J Nucl Med* 1985;10:341–345.
43. Berry JJ, Baker JA, Pieper KS, et al. The effect of metabolic milieu on cardiac PET imaging using fluorine-18-deoxyglucose an nitrogen-13-ammonia in normal volunteers. *J Nucl Med* 1991;32:1518–1525.
44. Fidler IJ. The biology of human cancer metastasis. *Acta Oncol* 1991;30:669–675.
45. Sasaki M, Ichiya Y, Kuwabara et al. Fluorine-18-fluorodeoxyglucose positron emission tomography in technetium-99m-hydroxymethylenediphosphonate negative bone tumors. *J Nucl Med* 1993;34:288–290.
46. Tahara T, Ichiya Y, Kuwabara Y, et al. High [^{18}F]-fluorodeoxyglucose uptake in abdominal abscesses: a PET study. *J Comput Assist Tomogr* 1989;13:829–831.
47. Sasaki M, Ichiya Y, Kuwabara Y, et al. Ringlike uptake of [F-18] FDG in brain abscess: a PET study. *J Comput Assist Tomogr* 1990;14:486–487.
48. Kubota R, Yamada S, Kubota K, et al. Intratumoral distribution of fluorine-18-fluorodeoxyglucose in vivo: high accumulation in macrophages and granulation tissue studied by microautoradiography. *J Nucl Med* 1992;33:1972–1980.
49. Kubota R, Kubota K, Yamada S, et al. Microautoradiographic study for the differentiation of intratumoral macrophages, granulation tissues and cancer cells by the dynamics of fluorine-18-fluorodeoxyglucose uptake. *J Nucl Med* 1994;35:104–112.
50. Kao CH, Wang SJ, Liu TJ. The use of technetium-99m-metoxyisobutylisonitrile breast szintigraphy to evaluate palpaple breast masses. *Eur J Nucl Med* 1994;21:432–436.
51. Aktolun C, Bayhan H, Kir M. Clinical experience with ^{99m}Tc-MIBI imaging in patients with malignant tumors. Preliminary results and comparison with ^{201}Tl. *Clin Nucl Med* 1992;17:171–76.
52. Kaiser WA, Zeitler E. MR imaging of the breast: fast imaging sequences with and without GD DTPA. *Radiology* 1989;170:681–86.
53. Heywang SH, Wolf A, Pruss E, Hilbertz T, Eiermann W, Permanetter W. MR imaging of the breast with GD-DTPA: use and limitations. *Radiology* 1989;171:95–103.

Dynamic Indium-111-Pentetreotide Scintigraphy in Breast Cancer

Marika Bajc, Christian Ingvar and John Palmer
Departments of Clinical Physiology, Surgery and Radiophysics, Lund University, Lund, Sweden

The efficacy of imaging breast cancer with ^{111}In-pentetreotide (somatostatin receptor scintigraphy) was evaluated before surgery. **Methods:** Seventy-one whole-body scintigrams in 24 patients with known breast cancer and 24 whole-body scintigrams in 8 controls were obtained at 0.5, 5 and 24 hr after intravenous injection of 110 MBq ^{111}In-pentetreotide. Anterior and posterior projection images were acquired simultaneously. SPECT of the thorax was performed at 5 or 24 hr after injection in all breast cancer patients. The specimens were imaged immediately after surgery and the distribution of pentetreotide was assessed qualitatively and quantitatively. **Results:** Somatostatin receptor-positive tumors were found in 18/24 patients with breast cancer. Pentetreotide uptake was significantly greater in breast cancer patients compared to control patients. In all patients with positive images, the early scintigram (0.5 hr) showed abnormal uptake. It was possible to delineate three different dynamic patterns. Increased uptake was visually most distinct either at 0.5 hr (4 patients) or at 5 hr (5 patients), or equally distinct at each time (9 patients). Moreover, bilaterally increased pentetreotide uptake was observed in 10/18 true-positive patients (in 8 at each time and in 2 patients only at 5 hr), but only one patient had a known bilateral tumor. **Conclusion:** We found higher incidence of somatostatin receptors in patients with breast cancer than in the control group. Moreover, bilaterally increased pentetreotide uptake in clinically unilateral disease was an unexpected finding.

Key Words: breast cancer; indium-111-pentetreotide; dynamic imaging

J Nucl Med 1996; 37:622–626

Indium-111-pentetreotide scintigraphy has made it possible to visualize tumors expressing somatostatin receptors in vivo. The method has been established for diagnosis of gastrointestinal endocrine tumors (GEP) and has high sensitivity (*1*). In addition to neuroendocrine tumors, there are a variety of tumors in the lungs, lymphopoetic system, central nervous system and breasts which also express somatostatin receptors (*2–6*).

Nesland et al. (*7*) have argued that some breast tumors have neuroendocrine features. Moreover, Papotti et al. (*8*) have defined a group of breast carcinomas expressing neuroendocrine features and the presence of somatostatin receptors. Reubi et al. (*4*) measured in vitro somatostatin receptors and showed that approximately half of the breast cancer tumors possess specific receptors. Krenning et al. (*1*) and van Eijck et al. (*9*) used in vivo scintigraphy and observed an even higher incidence of somatostatin receptors (74%). The detection of breast tumors with somatostatin receptor imaging is of biological and potentially of therapeutic interest. Presence of somatostatin receptors may be a useful prognostic factor and may play an active role in regulating tumor development (*10*).

The aim of this study was to investigate whether breast cancer expresses somatostatin receptors. The relation of the somatostatin receptor to the histopathology and to estrogen (ER) or progesterone receptor (PgR) also was studied.

MATERIALS AND METHODS

Patients

Patients with invasive breast cancer detected by physical examination, mammography and cytology who were scheduled for surgery were studied. The study was approved by the Ethics and Isotope Committees at Lund University. The study group consisted of 22 women and 2 men; aged 36–83 yr (mean age 61 yr). One woman had a bilateral tumor. There was a total of 25 known breast tumors used in the study. Pentetreotide scintigraphy was started 48 hr before surgery. Eight patients with GEP tumors in the same age group undergoing pentetreotide scintigraphy served as controls.

Received Jan. 20, 1995; revision accepted Aug. 18, 1995.
For correspondence or reprints contact: Marika Bajc, MD, PhD, Department of Clinical Physiology, Lund University, University Hospital, S-221 85 Lund, Sweden.